International Journal of Signal Processing, Image Processing and Pattern Recognition
Vol.8, No.11 (2015), pp.165-178
http://dx.doi.org/10.14257/ijsip.2015.8.11.16

# Design of an Electrical Capacitance Tomography System based on LabVIEW

Y. G. Zhou[1], H. Yan[2] and Z. Fang[3]

*School of Information Science and Engineering,*
*Shenyang University of Technology, Shenyang, China*
*[1]zhouygok@126.com, [2] yanhua_01@163.com, [3] fzhzhimeng_1988@126.com*

***Abstract***

*Electrical capacitance tomography (ECT) is an effective technique for visualizing the distribution of dielectric materials inside a closed pipe or vessel. The design of an ECT system based on LabVIEW is described in this paper. The system can be divided into three parts: sensor system, data acquisition system, and imaging computer. The data acquisition system designed takes C8051F700 MCU as the core to acquire capacitance data. The computer implements the functions such as data processing, image reconstruction, image display and system control. Serial communication is used between the data acquisition system and the computer. LabVIEW, a graphical programming language, is chosen as the development environment. An optimal thresholding scheme is proposed which can reduce low grey-level artifacts effectively. Equipped with a classic ECT sensor or a direct 3D ECT sensor, the system designed can work in 2D reconstruction mode or direct 3D reconstruction mode. The software design in LabVIEW is focused on.*

***Keywords:*** *electrical capacitance tomography, image reconstruction, LabVIEW, Serial communication, image display*

## 1. Introduction

Tomographic techniques have been widely accepted as a valuable tool for process control and monitoring. Electrical Capacitance Tomography (ECT) offers some advantages over other tomography modalities, such as no radiation, rapid response, low-cost, being non-intrusive and non-invasive. ECT is aimed at visualizing the permittivity distribution in the interior of an enclosed environment by means of external capacitance measurements [1-2].

The classic ECT is to reconstruct a 2D image of a process cross section. Recently, 3D ECT has gained interest because of most processes taking place in 3D space. 3D ECT can be achieved in tow ways. The first (called 2.5D) is to use a few independent 2D images and to interpolate them into a 3D image. This method has been widely used in medical applications of tomography for many years already. The second method is direct 3D reconstruction, where sensor provides 3D measurements and a 3D image is directly obtained during the reconstruction process [3-6]. A direct 3D ECT sensor usually has at least two-plane measuring electrodes in axial direction. For a fixed number of electrodes, the increase of planes is countered by a decrease in radial resolution. In some publications, 3D ECT is also called electrical capacitance volume tomography (ECVT) [3-4, 7] due to the fact that it can realize volumetric imaging.

The design of an ECT system based on LabVIEW is given in this paper. Equipped with a classic ECT sensor or a direct 3D ECT sensor, it can work in 2D reconstruction mode or direct 3D reconstruction mode.

ISSN: 2005-4254 IJSIP

## 2. Composition of an ECT system

Usually, an ECT system consists of three basic components: (1) a multi-electrode capacitance sensor surrounded by an earthed screen; (2) a data acquisition system, including capacitance measuring circuits and a data acquisition unit and (3) an image computer for data processing, image reconstruction and image viewing, see Figure 1. The data acquisition system acquires the capacitance data between any electrode pairs and feed them into the computer. The computer reconstructs the permittivity distribution in the sensing region of the sensor from these data by using a reconstruction algorithm, and displays the distribution on the computer screen.

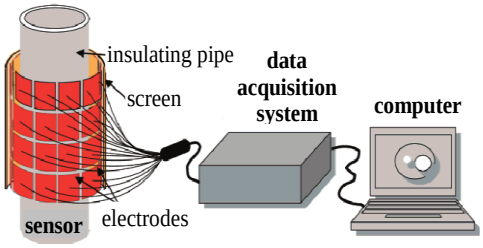


**Figure 1. Diagram of the ECT System**

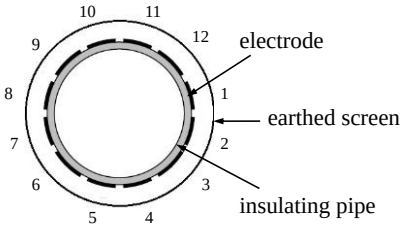


**Figure 2. Diagram of the Classic ECT System**

In a complete measurement cycle, a excitation potential is first supplied to electrode 1 (which is referred to as the source electrode) and the capacitances between 1 and 2, 1 and 3, …, and 1 and L (L is the number of electrodes) are measured. Next, electrode 2 is the source electrode and the capacitances between 2 and 3, 2 and 4, …, and 2 and L are measured. This process continues until electrode L-1 is the source electrode, and the capacitance between L-1 and L are measured [8-9]. In this way, a total of independent capacitance measurements are produced in a cycle.

Figure 2 and Figure 3 give the structure diagrams of the classic ECT sensor and the direct 3D ECT sensor used in our ECT system based on LabVIEW. Both sensors have 12 electrodes mounted symmetrically on the outside of an insulating pipe, and give 66 (L=12, M=66) independent capacitance measurements. The difference between the two sensors lies in electrode size and electrode layout. The electrodes of the direct 3D ECT sensor are short wide, arranged in three planes and every four electrodes on each plane are rotated 45 with reference to the previous one. In contrast, the electrodes of the classic ECT sensor are long narrow, arranged in the same plane.

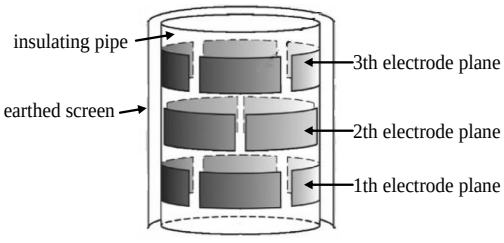


**Figure 3. Diagram of the direct 3D ECT system**

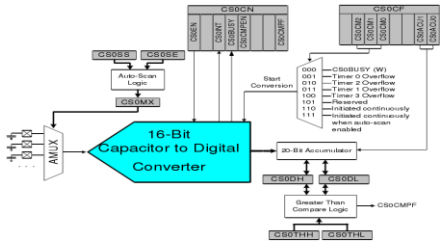


**Figure 4. Block Diagram of the Capacitance Sensing Subsystem**

In this paper, the data acquisition system takes C8051F700 MCU as the core to acquire capacitance data. C8051F700 integrated chip contains a capacitance sense subsystem (called CS0), whose core is a built-in 16-bit Capacitance to digital converter, see Figure 4.

CS0 uses the capacitance to digital converter to determine the capacitance on a port pin. CS0 can take measurements from different port pins using the its 32-channel analog multiplexer. CS0 is enabled only when the CS0EN bit (CS0CN) is set to 1. Otherwise CS0 is in a low-power shutdown state. CS0 can be configured to take measurements on one port pin or a group of port pins, using auto-scan. An accumulator can be configured to accumulate multiple conversions on an input channel. Interrupts can be generated when CS0 completes a conversion or when the measured value crosses a threshold defined in CS0THH:L. In order for a port pin to be measured by CS0, that port pin must be configured as an analog input. Configuring the input multiplexer to a port pin not configured as an analog input will cause the capacitive sense comparator to output incorrect measurements [10].

C8051F700 contains 32 capacitance input ports; each port can be connected with an electrode of the ECT sensor by a shielded cable. The measured capacitance value can be directly converted to 16-bit precision digital. In the working status, C8051F700 can select an electrode as the grounding electrode, and acquire the capacitance value between the grounding electrode and other electrodes all at once. After a selectable accumulation for de-noising, these data are fed into the PC through a USB to RS232 converter chip.

The electrical capacitance tomography system is designed based on Virtual Instrument Technology. LabVIEW, a graphical programming language, is chosen as the development environment for several reasons. It is a graphical rather than a text based programming language such as C or FORTRAN, allowing faster development. It allows the programming of complex functionality without knowledge of low-level routines: *e.g.*, setting up a TCP/IP socket. Another argument is the fast execution of the complied code (comparable to C-code). Finally the program easily integrates with existing hardware and/or external code [11-12].

The program written in LabVIEW is called VI, it contains two parts: a front panel and a graphical data flow diagram [12]. A front panel (*i.e.*, user interface) can both accept input from the user (sliders, knobs, values entered from the keyboard, push buttons, selector switches) and present output to the user (indicators, LEDs, graphs, strip charts, sounds). A LabVIEW program (called diagram) somewhat resembles the schematic for an electronic circuit. Wires represent variables that hold data. The various processes that act on these variables are represented by icons (small graphic objects that suggest the operation they perform). Graphical programming means that statements, variables and functions are represented by on-screen icons and ‘wires’, rather than by lines of text. In a LabVIEW program, execution is not controlled by the order in which the statements were written in the source code (line-oriented programming), but, rather, by the data that are generated (data flow oriented). For example, subroutines that use data originating from an A/D conversion board as input do not execute until the data have been acquired.

The front panel when the ECT system based on LabVIEW works in the 3D reconstruction mode is shown in Figure 5.

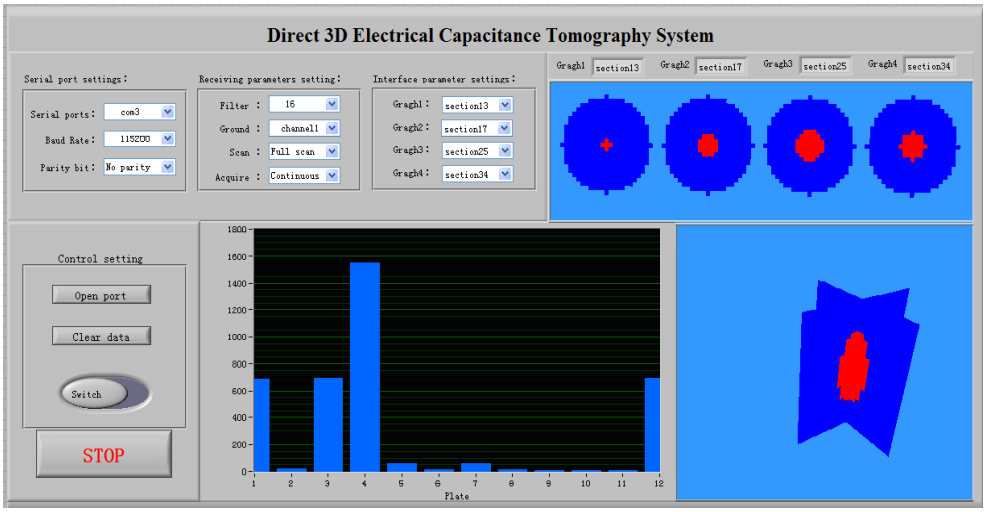


**Figure 5. Front Panel of Direct 3D Electrical Capacitance Tomography System**

## 3. Outline of Computer Software

The computer software of the ECT system is developed in LabVIEW. Communication module and reconstruction module are the two main modules of the software.

The communication module implements the acquisition and storage of capacitance data by the control of C8051F700 MCU and the communication with C8051F700 MCU. The communication module controls the running state of the MCU by selecting the grounding plate, the method of MCU scan and data acquisition. The capacitance data is acquired from C8051F700 MCU through a serial port and displayed intuitively in the screen in histogram form. Besides the real-time display of capacitance data, current capacitance data can be stored in a data text file named by time at the user's request for subsequent data analysis and processing.

The reconstruction module completes the mesh generation, image reconstruction, image display and other functions. The reconstruction module generates a Cartesian coordinates array cluster of the node points of the permittivity mesh elements, calculates the permittivity values corresponding to the capacitance data acquired from the communication module by using a user-selected image reconstruction algorithm, converts the permittivity value of each pixel into the RGB color series, and display the reconstructed image by filling pixels with their color series. The sensitivity matrix, the empty/full pipe capacitance values, and the node coordinate values of pixels for the image reconstruction are imported into the program in the form of text file.

Before taking capacitance measurements, it is necessary to calibrate an ECT system, to obtain capacitance values when the sensor is completely filled with a low permittivity material and a high permittivity material, respectively. These values are used to normalize the measured data for image reconstruction.

During measurement, a set of data, which is called one frame measurement data, is transmitted from the data acquisition unit to the image computer as a matrix called Capacitance. Then matrix Capacitance is used to generate a matrix called Estimated Permittivity by using a certain reconstruction algorithm, *e.g.*, the LBP algorithm [9-19]. Matrix Estimated Permittivity describes the 2D or 3D normalized permittivity distribution in the measured region. Its dimension is determined by the image resolution.

A continuous measurement process is to receive measurement results frame by frame and store them into a measurement data queue. In the meanwhile, using a certain reconstruction algorithm, a corresponding RGB color matrix for each frame is generated and stored into an image data queue. Both of the data queues are working as FIFO, which

 

can keep the data in sequence for a pre-assigned period. Figure 6 shows the basic data processing flow during measurement.

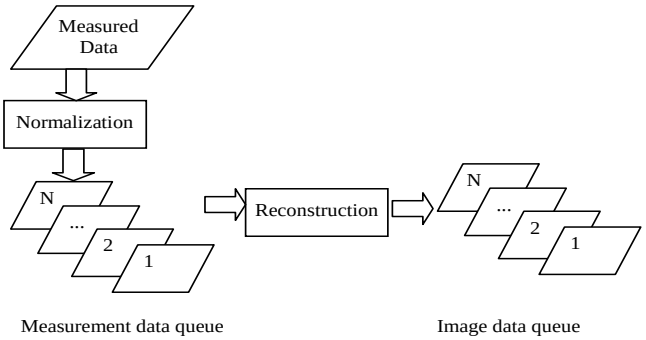


**Figure 6. Data Processing Flow**

## 4. Design of Key Software

### 4.1. Serial Port Communication

In the designed the ECT system based on LabVIEW, the communication between the image computer and the MCU is conducted by series port communication. Serial communication program is written by using VISA node. VISA is a standard I/O API for instrumentation programming. [19]VISA can control GPIB, serial, USB, Ethernet, PXI, or VXI instruments, making the appropriate driver calls depending on the type of instrument you use so you do not have to learn instrument-specific communication protocol.

The serial communication program used in this paper is shown in Figure 7. It implements serial communication as follows. First, initialize the serial port, that is, set serial port number, baud rate and other parameters by use 'VISA Configure Serial Port' for communication. Second, read and write the serial port, that is, according to the structure of data in the communication protocol, write control instruction into MCU by 'VISA Write' function to control the method of data acquisition; then read the data from MCU by 'VISA Read' function. Third, close the serial port, that is, close the serial port after the end of reading/writing serial port.

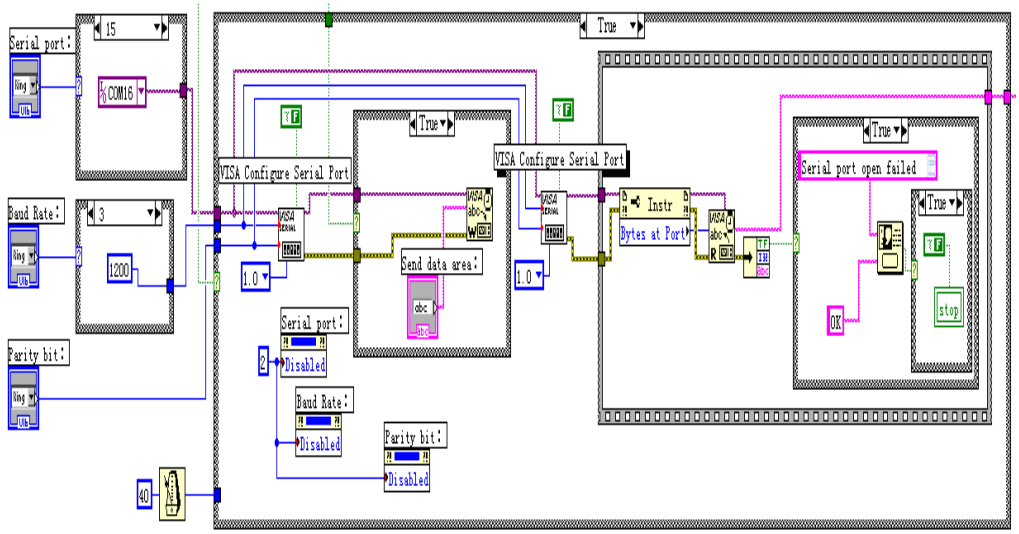


**Figure 7. Diagram of the Serial Communication Program**

### 4.2. Permittivity Reconstruction

When all the capacitance values for a complete frame are sampled, permittivity reconstruction is achieved by Permittivity Calculation subVI. [19]. To retrieve the dynamic material distribution within the sensing domain, the ECT systems remove the effect of background material by normalizing the raw capacitance data with the data measured in two special cases where the ECT sensor is full filled by the background material (low permittivity material with permittivity of $\varepsilon_l$), and by the material being monitored (high permittivity material with permittivity of $\varepsilon_h$). Suppose the corresponding capacitance values measured in these cases are $c_{ij}^{l}$ and $c_{ij}^{h}$, respectively, the normalized capacitance can be expressed as:

$$\lambda_{ij} = \frac{c_{ij} - c_{ij}^{l}}{c_{ij}^{h} - c_{ij}^{l}} \tag{1}$$

where $c_{ij}$ represents the capacitance of electrode pair *i-j* resulting by the material distribution to be imaged. In the VI design, the normalization is realized by the Data Normalization subVI as shown in Figure 8. The (*i.e.*, C_l in Figure 8) and (*i.e.*, C_h in Figure 8) are pre-loaded. In ECT, the relationship between the measured interelectrode capacitance and the permittivity distribution of the region to be reconstructed is nonlinear but, for simplicity, can be simplified to a linear form:

$$\begin{aligned} &\boldsymbol{\lambda} = \boldsymbol{S}\boldsymbol{g} \\ &\boldsymbol{\lambda} = [\lambda_{12}\ \lambda_{13}\ \cdots\ \lambda_{1L}\ \lambda_{23}\ \cdots\ \lambda_{(L-1)L}] \\ &\boldsymbol{g} = [g_1\ g_2\ \cdots\ g_N]^T \end{aligned} \tag{2}$$

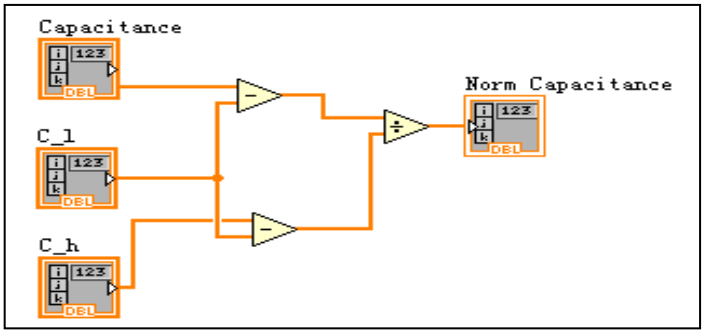


**Figure 8. Diagram of Data Normalization subVI**

Where, $\boldsymbol{\lambda}$ is the normalized capacitance vector, $\boldsymbol{g}$ is the normalized permittivity vector, and $\boldsymbol{S}$ is the Jacobian matrix of normalized capacitance with respect to the normalized permittivity, *i.e.*, the normalized sensitivity matrix. The normalized permittivity is often called normalized grey level, and g is often called grey vector too. The *k*th element of the normalized permittivity vector g is calculated as follows.

$$g_k = \frac{\hat{\varepsilon}_k - \varepsilon_l}{\varepsilon_h - \varepsilon_l} \tag{3}$$

where $\hat{\varepsilon}_k$ represents the reconstructed permittivity of the kth element.

The electrostatic field in ECT sensor is governed by Laplace's equation (assuming no free charge inside the screen) [8-9] and the associated boundary conditions (the Dirichlet conditions, *i.e.*, the known potentials of all the electrodes and the screen) imposed by the measurement technique. Since the permittivity distribution is very irregular, the finite element (FE) method [14-16] is used to obtain a numeric solution. That means the Jacobian matrix $\boldsymbol{S}$, in other word, the sensitivity maps can be obtained by FE analysis. Subdividing the image domain into N elements, the sensitivity of kth element of electrode pair i-j can be written as [14]:

$$s_{ij}(k) = \frac{c_{ij}(k) - c_{ij}^{l}}{c_{ij}^{h} - c_{ij}^{l}} \frac{1}{\varepsilon_h - \varepsilon_l} \mu(k)$$
$$i = 1, 2, ..., L-1,\ j = i+1, ...L,\ k = 1, 2, ..., N \tag{4}$$

where $c_{ij}(k)$ is the capacitance of electrode pair *i-j* when the *k*th element has permittivity $\varepsilon_h$ and all other elements have permittivity $\varepsilon_l$ ; $c_{ij}^{l}$ and $c_{ij}^{h}$ are the capacitances of electrode pair *i-j* when the imaging region is filled with material of permittivity $\varepsilon_l$ and $\varepsilon_h$ , respectively; in 2D reconstruction, $\mu(k) = A_{\max} / A_k$ , $A_k$ and $V_{\max}$ are the areas of the *k*th and maximum elements, respectively; in 3D reconstruction, $\mu(k) = V_{\max} / V_k$ , $V_k$ and $V_{\max}$ are the volumes of the kth and maximum elements, respectively.

The sensitivity matrix $\boldsymbol{S}$ in can be written as:

$$\boldsymbol{S} = \begin{bmatrix} s_{12}(1) & s_{12}(2) & \cdots & s_{12}(N) \\ s_{13}(1) & s_{13}(2) & \cdots & s_{13}(N) \\ \vdots & \vdots & \ddots & \vdots \\ s_{(L-1)L}(1) & s_{(L-1)L}(2) & \cdots & s_{(L-1)L}(N) \end{bmatrix} \tag{5}$$

In past years, various image reconstruction algorithms have been introduced for ECT image reconstruction [19]. At present, however, the LBP algorithm is still widely used for on-line image reconstruction because of its simplicity. Using LBP algorithm, the normalized permittivity vector can be calculated as follows:

$$\hat{\boldsymbol{g}} = \frac{\boldsymbol{S}^T \boldsymbol{\lambda}}{\boldsymbol{S}^T \boldsymbol{u}}, \boldsymbol{u} = [1, 1, ..., 1] \tag{6}$$

where $\boldsymbol{u}$ is an M×1 identity vector, The division of the two vector $\boldsymbol{S}^T\boldsymbol{\lambda}$ and $\boldsymbol{S}^T\boldsymbol{u}$ is defined as one numerator component being divided by the corresponding denominator component.

In the VI design, the LBP algorithm is realized by the Permittivity Calculation subVI as shown in Figure 9. The vector of normalized capacitance values (Norm Capacitance) is imported from the Data Normalization subVI. The Sensitivity Matrix (**S**) is pre-calculated and preloaded. The operation of matrix transpose, matrix multiplication, and numerical division in Equation (6) are realized by using the 2D Array Transpose, Matrix Multiplication, and number division modules as shown in Figure 9.

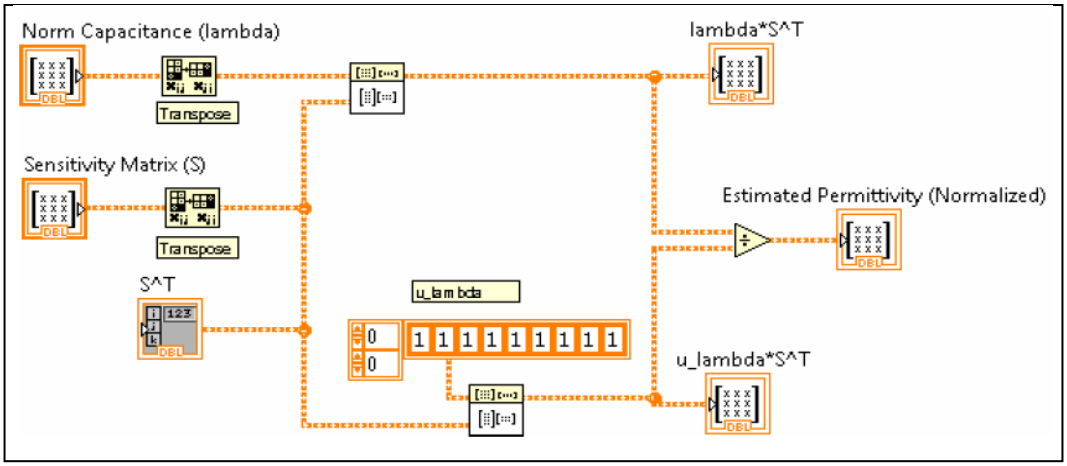


**Figure 9. Diagram of Permittivity Calculation subVI**

Although the LBP algorithm is widely used for on-line imaging, it can only provide qualitative images since many low grey-level artifacts exist in its reconstruction images [9, 13, 17, 19, 20]. In order to improve the reconstruction quality, an optimal thresholding scheme is proposed in this paper which can reduce artifacts effectively. Basically, the optimal threshold is obtained by considering all possible thresholds and choosing the threshold which has the minimum error from the measured values.

$$\min_i \left\| \boldsymbol{C} - \boldsymbol{S}\boldsymbol{g}_i \right\|_2^2 \tag{7}$$

Where $i \in 1, 2, \ldots 100$ is the *i*th discretized threshold, and the *k*th element of vector $\boldsymbol{g}_i$ can be calculated as:

$$\boldsymbol{g}_i(k) = \begin{cases} 1, & if\ \boldsymbol{g}(k) > i\text{th threshold} \\ 0, & else \end{cases} \tag{8}$$

where $\boldsymbol{g}(k)$ represents the grey level of the *k*th element in the reconstruction image. The process of finding optimal threshold η is very fast with 100 discretized threshold. Experiments have suggested that following threshold operation can reduce low grey-level artifacts effectively.

$$\boldsymbol{g}_i(k) = \begin{cases} 0, & if\ \boldsymbol{g}(k) < \eta \\ 1, & if\ \boldsymbol{g}(k) > 1 \\ \boldsymbol{g}(k), & otherwise \end{cases} \tag{9}$$

### 4.3. Image Generation in 2D Reconstruction Mode

When the permittivity distribution to be imaged is reconstructed, it is converted into an image representing the material permittivity distribution via Image Generation subVI. Figure 10 shows the block diagram of Image Generation subVI. The operation functions are built within a loop structure, the core of this subVI is the set of the mesh parameter attribute node of the reate Mesh subVI. In Figure 10, following subVIs are used. The Create Mesh.vi generates a Cartesian coordinate array cluster of the node points of the permittivity mesh elements.The 288.vi produces an array of ordinal numbers, used to identify the order of the elements in the mesh.

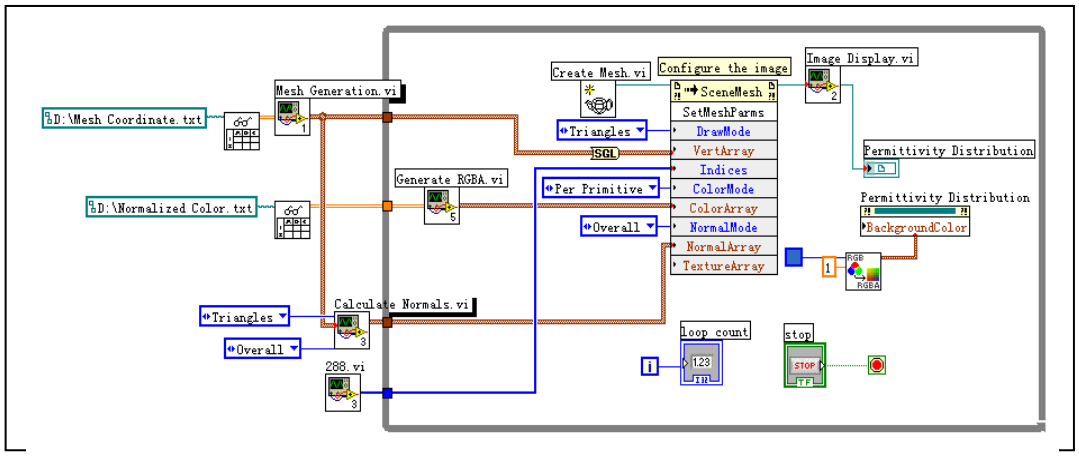


**Figure 10. Diagram of Image Generation subVI**

The Calculate Normal subVI is used to determine the normal vector array (NormalArray). It produces the vectors to be normal to the elements in the mesh; this should be uniform to avoid shading discrepancies. The Mesh Generation sub VI is used to generate the vertex array (VerArray). [19-20]The Generate RGBA subVI is used to generate color array (ColorArry).

The Create Mesh.vi generates a Cartesian coordinate array cluster of the node points of the permittivity mesh elements. The 288.vi produces an array of ordinal numbers, used to identify the order of the elements in the mesh.

The Calculate Normal subVI is used to determine the normal vector array (NormalArray). It produces the vectors to be normal to the elements in the mesh; this should be uniform to avoid shading discrepancies.The Mesh Generation sub VI is used to generate the vertex array (VerArray). The Generate RGBA subVI is used to generate color array (ColorArry).

The Image Display subVI is used to operate on the output of the mesh parameter attribute node to set site, size, light source, display interface background and so on. After above operations are completed, an image that displays the distribution of permittivity in the measured domain is generated [19]. The locations of all pixels are prewritten into the file named Mesh coordinate.txt. These coordinates are imported into the LabVIEW program by the File Read block, and then converted into a 2-dimentional array, Mesh Element Array, which is readable by the Image Generation subVI.

Figure 11 gives the diagram of Image Display subVI. The image variables created by the Image Generation subVI, including coordinates of the nodes as well as the color set for each pixels, are finally processed by the Image Display subVI to show the permittivity distribution on the screen. As shown in Figure 11, a total of 6 Invoke Nodes are employed to combine the image variables into a data flow. The image variables are read via Invoke Node 1 and 2 as the drawable attributes in a 3D workspace. The Invoke Node 3 and 5 set up a ring in gray color to represent the dimension of the pipe container. The direction and diffuse color of the virtual light source are set by Invoke Node 4 and 6. The color map of the permittivity distribution is finally displayed by a Graphic Indicator in the front panel as shown in Figure 11.

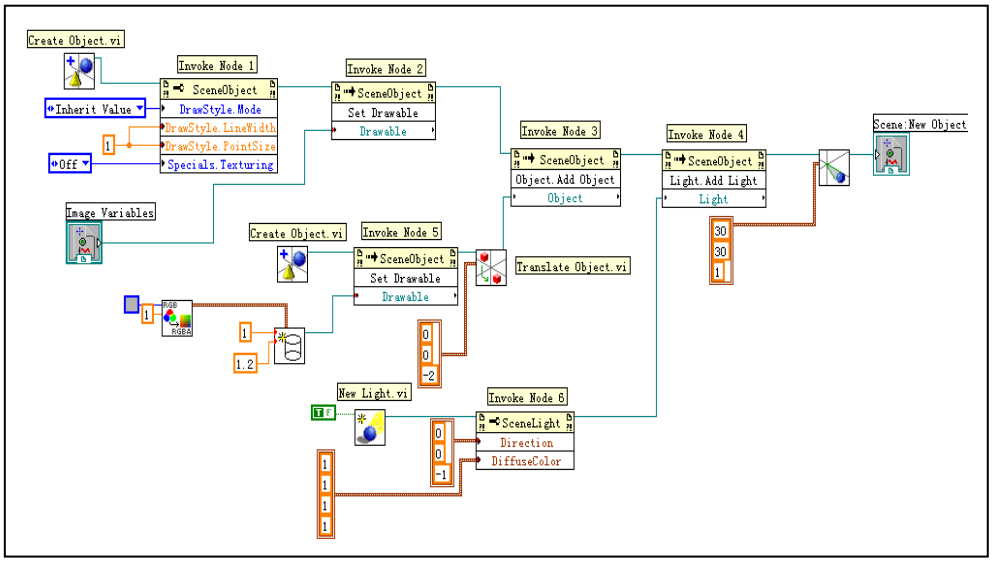


**Figure 11. Diagram of Image Display subVI**

In our system, the high material is displayed in red, while the low material is displayed in blue. The Perm2Color subVI converts the normalized permittivity value (*i.e.*, the grey value) of each pixel into the RGB (Red, Green, Blue, 0~255) color series. To highlight the interface between the two different materials, the permittivity close to mid-point $0.45<\boldsymbol{g}_t(k)\le 0.55$ is displayed in yellow. The corresponding permittivity-to-color conversion can be expressed as:

$$\begin{cases} R_k = 255 \\ G_k = \dfrac{1-\boldsymbol{g}_t(k)}{1-0.55}\cdot 255, \text{when } 0.55<\boldsymbol{g}_t(k)\le 1 \\ B_k = 0 \end{cases} \tag{10}$$

$$\begin{cases} R_k = \dfrac{\boldsymbol{g}_t(k)-0.45}{0.55-0.45}\cdot 255 \\ G_k = 255 \qquad \text{when } 0.45<\boldsymbol{g}_t(k)\le 0.55 \\ B_k = \dfrac{0.55-\boldsymbol{g}_t(k)}{0.55-0.45}\cdot 255, \end{cases} \tag{11}$$

$$\begin{cases} R_k = 255 \\ G_k = \dfrac{1-\boldsymbol{g}_t(k)}{1-0.55}\cdot 255, \text{when } 0.55<\boldsymbol{g}_t(k)\le 1 \\ B_k = 0 \end{cases} \tag{12}$$

After obtaining the RGBA color series, the normalized color series are written into the file named Normalized Color.txt. Figure 12 gives two examples of 2D image displays.

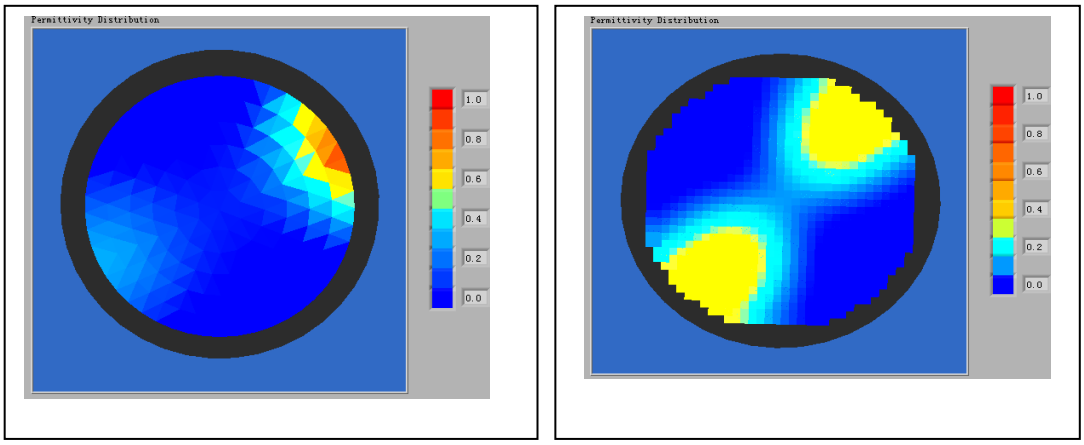


**Figure 12. Examples of 2D image displays**

### 4.4. Image Generation in 3D Reconstruction Mode

A very important step of the reconstruction process is to present reconstruction results and show them in a suitable and realistic form. The reconstruction result of direct 3D ECT is the 3D distribution of the material (permittivity). In this paper, slice planes are used to present the 3D distribution. Four cross-sections at different axial positions (z=constant) and a section obtained by x=0 and y=0 are used to illustrate the permittivity distribution reconstructed. Figure 5 shows the PC software interface, *i.e.*, the front panel of the ECT system written in LabVIEW. The interface includes two parts: control unit and display unit. In the control unit, a user can set the communication parameters, the acquisition method and choose four cross-sections from thirteen circular cross-sections. The display unit is divided into two display areas: the circular cross-section display and the cross-axial section display. Four images are presented in the circular cross-section display area; each image can be any of the thirteen circular cross-sections. Through these slice planes, the 3D distribution of the permittivity reconstructed can be well shown.

Figure 13 gives an example of the image displays for a 3D distribution. [18] The true 3D objects are given in the top of Figure 13, and the slice images displayed in the front panel of the ECT system based on LabVIEW are given in the bottom of Figure 13.

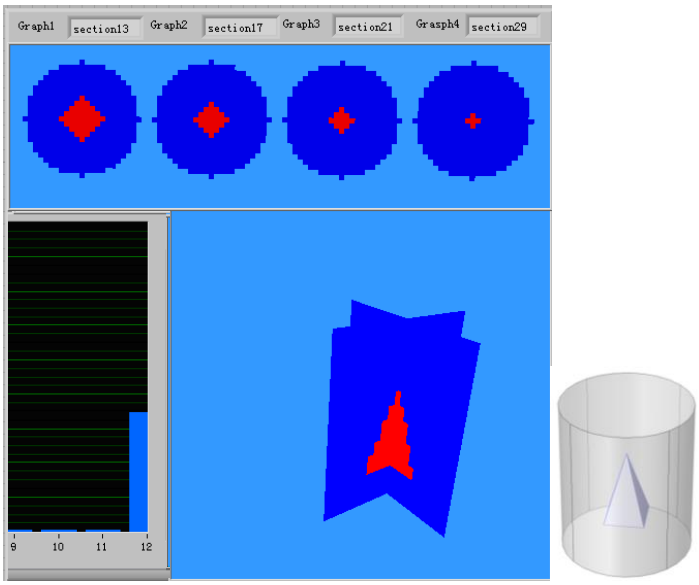


**Figure 13. Examples of 3D Image Displays**

## 5. Conclusion

Electrical capacitance tomography is one of the widely used techniques for monitoring the material distribution within an enclosed container. This paper presents the development of an electrical ECT system based on Virtual Instrument Technology. Since the system adopts LabVIEW as the software developing platform, takes C8051F700, a capacitive sensing mixed-signal MCU, as the core to acquire the capacitance data of all electrode pairs, the system developed is simple in structure, low in cost, good in industrial environment adaptation and easy in remote monitoring.

To obtain a large number of solutions from a relatively small number of measurements is inherently an undetermined problem. The selection of the number of pixels is a trade-off. Defining more pixels make the solution more undetermined. While the use of too few pixels will result in coarse images. Further investigation is needed in order to determine the optimal number of pixels for a particular application.

## Acknowledgment

This work is supported by National Natural Science Foundation of China (grant no. 61071141) and the Program for Liaoning Excellent Talents in University (grant no. LR2013005).

## References

[1] W. Q. Yang, "Design of electrical capacitance tomography sensors", Meas. Sci. Technol., vol.21, February 2010, doi:10.1088/0957-0233/21/4/04, **(2001).**
[2] A. J. Jaworski and T. Dyakowski, "Application of electrical capacitance tomography for measurement of gas–solids flow characteristics in a pneumatic conveying system", Meas. Sci. Technol., vol.12, (**2001),** pp.1109–1119.
[3] W. Warsito, Q. Marashdeh and L. S. Fan L S, "Electrical capacitance volume tomography", IEEE Sens. J., vol. 7, (**2007**), pp. 525–535.
[4] F. Wang, Q. Marashdeh, L. S. Fan and W. Warsito, "Electrical capacitance volume tomography: design and applications," Sensors, vol.10, **(2010),** pp.1890–1917.
[5] R. Banasiak, R. Wajman and D. Sankowski, "Three-dimensional nonlinear inversion of electrical capacitance tomography data using a complete sensor model", Progress In Electromagnetics Research, vol.100, **(2010)**, pp. 219–234.
[6] R. Wajman, P. Fiderek, H. Fidos, T. Jaworski, J. Nowakowski, D. Sankowski and R. Banasiak, "Metrological evaluation of a 3D electrical capacitance tomography measurement system for two-phase flow fraction determination", Meas. Sci. Technol., vol. 24, (**2013)** June, doi:10.1088/0957-0233/24/6/065302.
[7] Weber M. J., and Mei S. J., "Bubbling fluidized bed characterization using electrical capacitance volume tomography (ECVT)", Powder Technology, vol. 242, no.7, **(2013)**, pp. 40-50.
[8] H. Yan, L. J. Liu, H. Xu, and F. Q. Shao, "Image reconstruction in electrical capacitance tomography using multiple linear regression and regularization", Meas. Sci. Technol., vol.12, **(2001)**, pp. 575-581.
[9] C. G. Xie, S. M. Huang, B. S. Hoyle, R. Thorn, C. Lenn, D. Snowden and M. S. Beck, "Electrical capacitance tomography for flow imaging: system model for development of image reconstruction algorithms and design of primary sensors", IEE Proc. G, vol.139, **(1992)**, pp. 89–98.
[10] http://www.soiseek.cn/ic/SILABS/C8051F71X/1.html C8051F70x/71x.pdf.
[11] M. Dierick, B. Masschaele and V. L. Hoorebeke, "Octopus, a fast and user-friendly tomographic reconstruction package developed in LabView", Meas. Sci. Technol., vol. 15, **(2004)**, pp. 1366–1370.
[12] L. Wang, Proficient in Labview 8.X. Beijing: Electronic Industry Press, **(2008).**
[13] W. Q. Yang and L. H. Peng, "Image reconstruction algorithms for electrical capacitance tomography", Meas. Sci. Technol., vol.14, (**2003)**, pp. R1–R14.
[14] H. Yan, F. Q. Shao, H. Xu and S. Wang, "Three-dimensional analysis of electrical capacitance tomography sensing fields", Meas. Sci. Technol, vol.10, no.8, (**1999**), pp. 717-725.
[15] Z. G. Wang, S. P. Peng and T. Liu, "GPU accelerated 2-D staggered-grid finite difference seismic modeling", Journal of Software, vol. 6, no. 8, **(2011)**, pp. 1554-1561.
[16] Z. F. Ming, T. Wen and T. Chen, "The simulation of electromagnetic suspension system based on the finite element analysis", Journal of Computers, vol. 8, no. 2, **(2013)**, pp. 308-312.
[17] Y. Li and D. J. Holland, "Fast and robust 3D electrical capacitance tomography", Meas. Sci. Technol., 105406(10pp), vol. 24, no. 10, **(2013)**.

 

[18] H. Yan, Y. Lu, and Y.F. Wang, "3D reconstruction and visualization of volume data in electrical capacitance Tomography", Journal of Software, vol. 8, no. 10, **(2013)**, pp. 2529-2534.
[19] Z.Y. Fan, R.X. Gao and J.J. Wang, "Virtual Instrument for Online Electrical Capacitance Tomography", practical applications and Solutions Using LabVIEW™ software, Dr. Silviu Folea (Ed.), (**2011)** August 1.
[20] Z. Zhao and R. Bai, "A fmcw radar distance measure system based on labview," Journal of Computers, vol. 6, no. 4, **(2011)**, pp. 747–754.

## Author

**Zhou Yinggang** received the B.Sc. degree (with distinction) in the measurement and control technology and instrument and the M. Eng. degrees in measurement technology and automatic devices from Shenyang University of Technology, Shenyang, China, in 1994 and 2003, now doctor. He is currently a Lecturer with the School of information in Shenyang University of Technology, Shenyang, China. His interests include process tomography, multiphase flow measurement, and inverse problems.